Conical diffraction in honeycomb lattices

Mark J. Ablowitz, Sean D. Nixon, and Yi Zhu*
Department of Applied Mathematics, University of Colorado, 526 UCB, Boulder, Colorado 80309-0526, USA
(Received 16 March 2009; published 18 May 2009)

Conical diffraction in honeycomb lattices is analyzed. This phenomenon arises in nonlinear Schrödinger equations with honeycomb lattice potentials. In the tight-binding approximation the wave envelope is governed by a nonlinear classical Dirac equation. Numerical simulations show that the Dirac equation and the lattice equation have the same conical diffraction properties. Similar conical diffraction occurs in both the linear and nonlinear regimes. The Dirac system reveals the underlying mechanism for the existence of conical diffraction in honeycomb lattices.

DOI: 10.1103/PhysRevA.79.053830 PACS number(s): 42.65.Tg, 42.70.Qs

I. INTRODUCTION

Conical diffraction is a fundamental feature of crystal optics and is of interest in mathematics and physics. Conical diffraction is the mechanism under which a narrow beam entering a biaxial crystal along its optic axis spreads into a hollow cone within the crystal. This phenomenon was first predicted by Hamilton [1] in 1832 and observed by Lloyd [2] soon afterward. It has been studied as a linear phenomenon experimentally and theoretically over the years [3,4]. We also note that conical diffraction in a nonlinear crystal has recently been investigated [5]. A key property associated with conical diffraction is the existence of the so-called diabolical points where two different dispersion surfaces touch each other. Interestingly the conical diffraction phenomenon also exists in the light beam propagation in honeycomb lattices as shown in recent work both experimentally and numerically [6–8].

It is well known that the material graphene has a honeycomb lattice structure. In the graphene literature, it has been shown that two different energy bands can touch each other at certain isolated points which are called Dirac points, i.e., such Dirac points are diabolical points. Thus diabolical points also exist in the band structure of two-dimensional (2D) honeycomb lattices. Moreover the structure of the dispersion relation near these Dirac points is conical in nature [9,10]; the regions in the neighborhood of the Dirac points are called Dirac cones. A remarkable effect associated with the Dirac points (diabolical points) in graphene is the quantum Hall effect [11]. A Dirac equation was used to describe this effect [12]. In optics, analogs of quantum Hall effect in honeycomb photonic crystals have been studied and the linear Dirac system has been derived from the Maxwell equation in a crystal [13,14]. However, no physical phenomena have been observed based on those analogs.

Similar to optics, Bose-Einstein condensation (BEC) can have lattice backgrounds and they are both governed by lattice nonlinear Schrödinger (NLS) equations. Recently, a nonlinear Dirac equation describing a weakly interacting bosonic gas in the presence of a honeycomb optical lattice for BEC [15] was derived. The Dirac points in BEC are thus diabolical points.

In this paper we derive the evolution equations for the wave envelope of the Bloch modes in the vicinity of diabolical points directly from the lattice nonlinear Schrödinger equation; a similar derivation can also be employed on the nonlinear optical Helmholtz equation. It turns out that the governing equation is a classical nonlinear Dirac system, consistent with the derivation via Hamiltonian methods in BEC [15] (see also investigations of the nonlinear Dirac system in [16]). The linear part of the Dirac system yields a dispersion relation which is the same as that obtained from the two-dimensional wave equation; this is the same dispersion relation as that of crystal optics [3] and helps explain why the beam propagates in a conical manner. This is further supported by simulations of the Dirac and lattice NLS equations and it is found that the same conical diffraction phenomena occur in both systems. Thus we associate the conical diffraction phenomena in honeycomb lattices with Dirac-type systems. In fact we find conical diffraction in both the linear and nonlinear Dirac systems.

The equation that describes a light beam propagating in a 2D lattice is the lattice nonlinear Schrödinger equation

$$i\psi_z + \nabla^2\psi - V(\mathbf{r})\psi + \sigma|\psi|^2\psi = 0. \tag{1}$$

Here σ, the coefficient of nonlinear term, is positive for focusing nonlinearity and negative for defocusing nonlinearity; $V(\mathbf{r})$ is the 2D periodic potential and $\mathbf{r}=(x,y)$. In photonic lattices, a model which has also been widely used is the saturable lattice NLS equation (cf. [17]). While the analysis on the lattice NLS equation below employs a linear potential and cubic nonlinearity, it can be readily extended to a saturablelike potential term.

II. BAND STRUCTURE OF THE HONEYCOMB LATTICES

The potential $V(\mathbf{r})$ we study is a honeycomb lattice. In this lattice, the local minima that we call sites form hexagons. The hexagonal lattice is usually generated by interacting three plane waves. We take the following lattice potential as our prototype:

$$V(\mathbf{r}) = V_0\left|e^{ik_0\mathbf{b}_1\cdot\mathbf{r}} + e^{ik_0\mathbf{b}_2\cdot\mathbf{r}} + e^{ik_0\mathbf{b}_3\cdot\mathbf{r}}\right|^2, \tag{2}$$

where $\mathbf{b}_1=(0,1)$, $\mathbf{b}_2=(-\frac{\sqrt{3}}{2},-\frac{1}{2})$, and $\mathbf{b}_3=(\frac{\sqrt{3}}{2},-\frac{1}{2})$; $V_0>0$ is the lattice intensity. This $V(\mathbf{r})$ is a honeycomb lattice with

*yi.zhu@colorado.edu

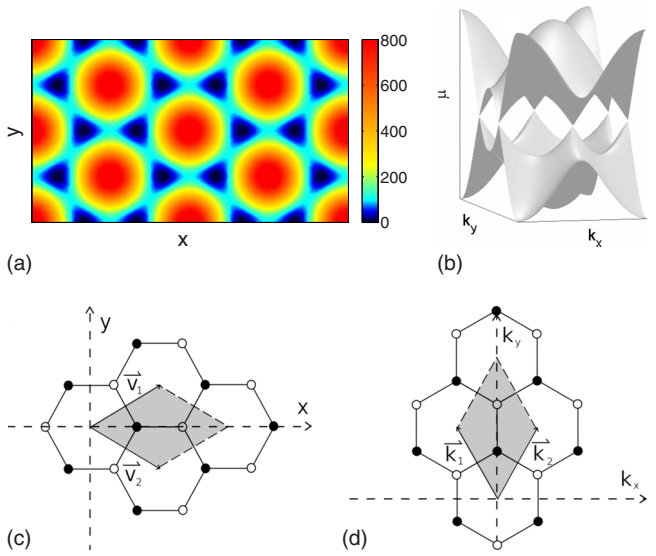

FIG. 1. (Color online) (a) The honeycomb lattice and (b) its first two bands. (c) The physical lattice and (d) reciprocal lattice are depicted. Shadow regions in the lattice and reciprocal lattice are the unit cell Ω and Brillouin zone Ω'.

intensity minima at the hexagonal vertices. The lattice has two periods (primitive lattice vectors)

$$\mathbf{v}_1 = \sqrt{3}l\left(\frac{\sqrt{3}}{2}, \frac{1}{2}\right), \quad \mathbf{v}_2 = \sqrt{3}l\left(\frac{\sqrt{3}}{2}, -\frac{1}{2}\right), \tag{3}$$

where $l=\frac{4\pi}{3\sqrt{3}k_0}$ is the lattice constant which is the distance of two nearest minima, i.e., $V(\mathbf{r}+m\mathbf{v}_1+n\mathbf{v}_2)=V(\mathbf{r})$ for any integers m and n. The unit cell Ω is the parallelogram with $\mathbf{v}_1$ and $\mathbf{v}_2$ as its two sides (cf. Fig. 1).

The band structure of this honeycomb lattice can be obtained from the linear lattice equation, i.e., Eq. (1) omitting the nonlinear term

$$i\phi_z + \nabla^2\phi - V(\mathbf{r})\phi = 0. \tag{4}$$

The Bloch modes follow from $\phi=e^{-i\mu z}u(\mathbf{r})$; substituting this into Eq. (4) one finds the eigenproblem

$$\mu u + \nabla^2 u - V(\mathbf{r})u = 0. \tag{5}$$

It is well known that the Bloch mode has the form $u(\mathbf{r};\mathbf{k})=e^{i\mathbf{k}\cdot\mathbf{r}}U(\mathbf{r};\mathbf{k})$ where $U(\mathbf{r};\mathbf{k})$ has the same periodicity as the potential $V(\mathbf{r})$; $\mathbf{k}=(k_x,k_y)$ is the wave number and the dispersion surface $\mu(\mathbf{k})$ has two periods,

$$\mathbf{k}_1 = \frac{4\pi}{3l}\left(\frac{1}{2}, \frac{\sqrt{3}}{2}\right), \quad \mathbf{k}_2 = \frac{4\pi}{3l}\left(\frac{1}{2}, -\frac{\sqrt{3}}{2}\right). \tag{6}$$

$\mathbf{k}_1$ and $\mathbf{k}_2$ are referred to as the reciprocal-lattice vectors which describe the Brillouin zone Ω'. They satisfy $\mathbf{v}_i\cdot\mathbf{k}_j=2\pi\delta_{ij}$. It is also noted that $u(\mathbf{r};\mathbf{k})$ is periodic with respect to $\mathbf{k}$.

Eigenproblem (5) can be solved numerically; this determines the dispersion relation (band structure). Typical bands 1 and 2 are displayed in Fig. 1(b). It is seen that the first and second bands touch each other at certain isolated points and these so-called diabolical points also display a honeycomb structure in the $\mathbf{k}$ plane. These diabolical points can be viewed as edges of a hexagonal region in the reciprocal lattice corresponding to the original potential lattice.

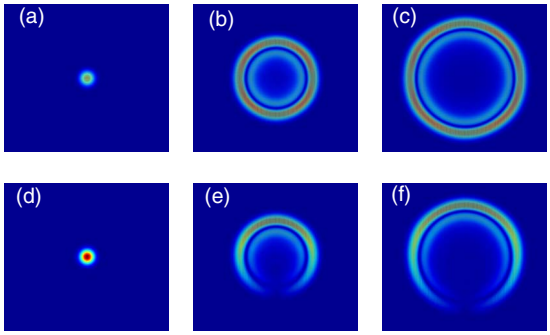

FIG. 2. (Color online) The propagation of Bloch modes associated with a diabolical point; (a)–(c) two plane waves; (d)–(f) one plane wave, each is multiplied by a Gaussian envelope.

There are two minima (sites) in a cell for the honeycomb lattice which we denote as A and B. All A sites or B sites differ spatially by multiples of $\mathbf{v}_1$ and $\mathbf{v}_2$. The A and B sites form two different triangular lattices: the A sublattice and B sublattice. In the reciprocal lattice, there are also two diabolical points in the first Brillouin zone which we call K and K'. They are depicted in Fig. 1(d). All dots are equivalent to K while all circles are equivalent to K'. For potential (2), $K=(0,\frac{4\pi}{3\sqrt{3}l})$ and $K'=(0,\frac{8\pi}{3\sqrt{3}l})$.

III. WAVE PROPAGATIONS IN THE HONEYCOMB LATTICES

We begin by studying the wave propagation in the honeycomb lattice numerically in Eq. (1). In order to understand the essential aspects of conical diffraction which has so far been observed to be a linear phenomenon, we first study the linear regime, i.e., $\sigma=0$. Later we will discuss results for the nonlinear regime, $\sigma=1$. In our simulations, $V_0=100$, $l=\frac{\pi}{24}$. Equation (1) is numerically integrated by the pseudospectral method coupled with the fourth-order Runge-Kutta integration in the time direction. We simulate the propagation of a wave envelope of Bloch modes near the diabolical point K. One can obtain the Bloch modes numerically and multiply the modes by a wide Gaussian envelope and use this wave packet as the initial beam. Alternatively, one can use one or more plane waves to excite the Bloch modes which are also experimentally accessible (see [6,18]). In order to compare with the previous work, here we only display the results with the second method. The simulations with both methods are consistent. We use two initial input beams. The first one is a Gaussian envelope multiplied by the sum of two plane waves for which the $\mathbf{k}$ vectors are two opposite diabolical points K and K'. The evolution is displayed in Figs. 2(a)–2(c). It is seen that an initial bell-shaped structure transforms into a ring structure after some distance. The ring structures contain two bright rings. The outer one is higher than the inner one. Between two bright rings is a dark ring. This dark ring is called Poggendorff's dark ring [3]. The second initial beam is a Gaussian envelope multiplied by one plane wave of

which the $\mathbf{k}$ vector is the diabolical point K. The results are displayed in Figs. 2(d)–2(f). The patterns are similar—a spot becomes two bright rings. However, the rings in the second simulation are not complete rings; they have notches at the bottom. The ring structures with notches are termed "half turn of polarization around the ring," which was also predicted by Hamilton and observed by Lloyd [3]. In both cases, the rings expand radially, but the width of the ring remains the same under propagation with decreasing intensity. As a result, one can see a cone in the lattice. This is exactly the so-called conical diffraction.

IV. DERIVATION OF THE DIRAC SYSTEMS

Next, we derive the governing equations for the propagation of the Bloch-mode envelopes. The Bloch mode $u(\mathbf{r};\mathbf{k})=e^{i\mathbf{k}\cdot\mathbf{r}}U(\mathbf{r};\mathbf{k})$ is periodic with respect to $\mathbf{k}$, so it can be expanded as a Fourier series

$$u(\mathbf{r};\mathbf{k})=\sum_{m,n} w_{m,n}(\mathbf{r})e^{-im\mathbf{k}\cdot\mathbf{v}_1-in\mathbf{k}\cdot\mathbf{v}_2}, \tag{7}$$

where $w_{m,n}(\mathbf{r})=\frac{1}{|\Omega'|}\int_{\Omega'}u(\mathbf{r};\mathbf{k})e^{-im\mathbf{k}\cdot\mathbf{v}_1-in\mathbf{k}\cdot\mathbf{v}_2}d\mathbf{k}$ is the so-called Wannier function. Here Ω' is the Brillouin zone, i.e., the unit cell in the $\mathbf{k}$ plane. From the definition, one has that $w_{m,n}(\mathbf{r})=w_{0,0}(\mathbf{r}-R_{m,n})$ where $R_{m,n}=m\mathbf{v}_1+n\mathbf{v}_2$ denotes the position of the cell with indices (m,n). Sometimes the subscripts are omitted and the Wannier function is referred to as $w(\mathbf{r}-R_{m,n})$ which for large V_0 is localized and centered around $R_{m,n}$ for special values of $\mathbf{k}$.

Since μ is also periodic in the $\mathbf{k}$ plane, one can also represent it as a Fourier series,

$$\mu(\mathbf{k})=\sum_{m,n}\mu_{m,n}e^{-im\mathbf{k}\cdot\mathbf{v}_1-in\mathbf{k}\cdot\mathbf{v}_2}. \tag{8}$$

Due to the properties of Wannier functions, any solution of Eq. (1) has the form

$$\psi(\mathbf{r},z)=\sum_{m,n,\alpha} C_{m,n,\alpha}(z)w_\alpha(\mathbf{r}-R_{m,n})e^{-i\mathbf{k}\cdot R_{m,n}}. \tag{9}$$

Here $R_{m,n}$ stands for the position of the cell with indices (m,n) and α is the index of different bands. In this paper, we only deal with the cases under which the components of higher bands are small, so only the first band expansion will be used. Thus, we discard the summation over α.

The above discussion is valid for any 2D periodic lattice. However, the lattices we are dealing with in this paper are honeycomb lattices which have certain unique features. A key feature of a honeycomb lattice is that it contains two minima (sites A and B, dot and circle in Fig. 1, respectively) in the unit cell. In tight-binding approximations, the honeycomb lattice can be broken up into two triangular sublattices: A and B lattices. In this case near a diabolical point, due to the degeneracy of the honeycomb lattice, expansion (9) can be written in the form

$$\psi(\mathbf{r},z)=\sum_{m,n} a_{m,n}(z)\tilde{w}(\mathbf{r}-A_{m,n})e^{-i\mathbf{k}\cdot A_{m,n}} + \sum_{m,n} b_{m,n}(z)\tilde{w}(\mathbf{r}-B_{m,n})e^{-i\mathbf{k}\cdot B_{m,n}}. \tag{10}$$

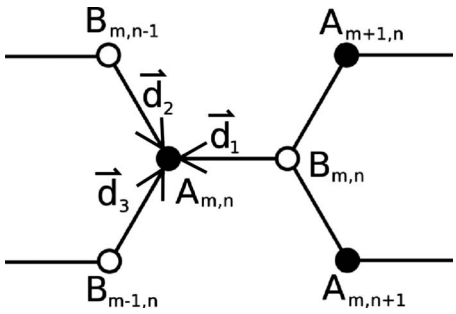

FIG. 3. The construction of the A and B lattices.

Here $A_{m,n}$ and $B_{m,n}$ are the site positions of the sublattices and $\tilde{w}(\mathbf{r})$ is the Wannier function associated with either of the triangular sublattices; it is localized and centered around the origin. The difference of the two sublattices is just a spatial shift $l(1,0)$. The Wannier functions of two sublattices, determined by the local properties around the sites of the potential, are the same. Here $A_{m,n}=A_{0,0}+m\mathbf{v}_1+n\mathbf{v}_2$ and $B_{m,n}=B_{0,0}+m\mathbf{v}_1+n\mathbf{v}_2$. We define three useful vectors: $\mathbf{d}_1=A_{m,n}-B_{m,n}=l(-1,0)$, $\mathbf{d}_2=A_{m,n}-B_{m,n-1}=l(\frac{1}{2},-\frac{\sqrt{3}}{2})$, and $\mathbf{d}_3=A_{m,n}-B_{m-1,n}=l(\frac{1}{2},\frac{\sqrt{3}}{2})$. The vectors and their relations are shown in Fig. 3.

Substituting Eqs. (8) and (9) into the lattice Eq. (1), we get

$$\sum_{m,n}\Bigg(i\frac{da_{m,n}}{dz}S_A(m,n)-\sum_{m',n'}\mu_{m',n'}a_{m-m',n-n'}S_A(m-m',n-n')e^{-i\mathbf{k}\cdot R_{m',n'}}+i\frac{db_{m,n}}{dz}S_B(m,n) - \sum_{m',n'}\mu_{m',n'}b_{m-m',n-n'}S_B(m-m',n-n')e^{-i\mathbf{k}\cdot R_{m',n'}}\Bigg) + \left(\sum_{m,n}a_{m,n}S_A(m,n)+b_{m,n}S_B(m,n)\right)^2 \times\left(\sum_{m,n}a_{m,n}S_A(m,n)+b_{m,n}S_B(m,n)\right)^*=0, \tag{11}$$

where, for convenience, we introduce the notation $S_A(m,n)=\tilde{w}(\mathbf{r}-A_{m,n})e^{-i\mathbf{k}\cdot A_{m,n}}$ and $S_B(m,n)=\tilde{w}(\mathbf{r}-B_{m,n})e^{-i\mathbf{k}\cdot B_{m,n}}$.

We can reduce Eq. (11) to an explicit discrete equation. We assume $|\mu_{0,0}|\gg|\mu_{m,n}|, m\neq 0$ or $n\neq 0$. This assumption is valid when the intensity of the potential is large ($V_0\gg 1$), i.e., the tight-binding approximation. The tight-binding approximation also relates Bloch functions to highly localized "Wannier functions" (cf. [19] for the tight-binding approximation associated with the one-dimensional NLS lattice equation). Then we can neglect long-range interaction terms in the linear part of Eq. (11) and only consider the nearest neighbors. In this context, we multiply Eq. (11) by a specific $S_A^*(\bar{m},\bar{n})$ (we drop the bar below) and integrate over the whole $\mathbf{r}$ plane and introduce ϵ, which is defined as

$$\epsilon = \frac{\int \tilde{w}^*(\mathbf{r} - A_{m,n})\tilde{w}(\mathbf{r} - B_{m,n})d\mathbf{r}}{\int |\tilde{w}(\mathbf{r} - A_{m,n})|^2 d\mathbf{r}}. \quad (12)$$

Notice that $w(\mathbf{r}-A_{m,n})$ is localized around $A_{m,n}$, so ϵ is small and, due to the properties of Wannier functions, is also independent of (m,n). Similarly, $\frac{\int \tilde{w}^*(\mathbf{r}-A_{m,n})\tilde{w}(\mathbf{r}-B_{m-1,n})d\mathbf{r}}{\int |\tilde{w}(\mathbf{r}-A_{m,n})|^2 d\mathbf{r}}$ and $\frac{\int \tilde{w}^*(\mathbf{r}-A_{m,n})\tilde{w}(\mathbf{r}-B_{m,n-1})d\mathbf{r}}{\int |\tilde{w}(\mathbf{r}-A_{m,n})|^2 d\mathbf{r}}$ are also small and are both equal to ϵ. We also assume $\epsilon\mu_{0,0}=O(1)$, which leads to a maximally balanced equation.

Keeping the dominant terms, we get

$$i\frac{da_{m,n}}{dz} - \mu_{0,0}a_{m,n} + g\sigma|a_{m,n}|^2 a_{m,n} - \epsilon\mu_{0,0}(b_{m-1,n}e^{i\mathbf{k}\cdot\mathbf{d}_3} + b_{m,n-1}e^{i\mathbf{k}\cdot\mathbf{d}_2} + b_{m,n}e^{i\mathbf{k}\cdot\mathbf{d}_1}) = 0, \quad (13)$$

where $\mathbf{d}_i$ are defined below Eq. (10) and $g=\frac{\int |\tilde{w}(\mathbf{r}-A_{m,n})|^4 d\mathbf{r}}{\int |\tilde{w}(\mathbf{r}-A_{m,n})|^2 d\mathbf{r}}$ which is also independent of (m,n); similarly, we can get

$$i\frac{db_{m,n}}{dz} - \mu_{0,0}b_{m,n} + g\sigma|b_{m,n}|^2 b_{m,n} - \epsilon\mu_{0,0}(a_{m+1,n}e^{-i\mathbf{k}\cdot\mathbf{d}_3} + a_{m,n+1}e^{-i\mathbf{k}\cdot\mathbf{d}_2} + a_{m,n}e^{-i\mathbf{k}\cdot\mathbf{d}_1}) = 0. \quad (14)$$

Here we are studying the propagation of a light beam with wave number $\mathbf{k}$ which is in the vicinity of diabolical points in the honeycomb lattice. The $\mathbf{k}$ in the above analysis is one of the diabolical points. We choose $\mathbf{k}=K=(0,\frac{4\pi}{3\sqrt{3}l})$.

Then we get the discrete equations

$$i\frac{da_{m,n}}{dz} - \mu_{0,0}a_{m,n} + g\sigma|a_{m,n}|^2 a_{m,n} - \epsilon\mu_{0,0}\left[b_{m-1,n}\left(-\frac{1}{2}+\frac{\sqrt{3}}{2}i\right) + b_{m,n-1}\left(-\frac{1}{2}-\frac{\sqrt{3}}{2}i\right) + b_{m,n}\right] = 0, \quad (15)$$

$$i\frac{db_{m,n}}{dz} - \mu_{0,0}b_{m,n} + g\sigma|b_{m,n}|^2 b_{m,n} - \epsilon\mu_{0,0}\left[a_{m+1,n}\left(-\frac{1}{2}-\frac{\sqrt{3}}{2}i\right) + a_{m,n+1}\left(-\frac{1}{2}+\frac{\sqrt{3}}{2}i\right) + a_{m,n}\right] = 0. \quad (16)$$

It should be noted that had we analyzed the lattice in the neighborhood of a different critical point in the lattice, a different discrete evolution equation would ensue. For example, in the neighborhood of centers the hexagonal reciprocal lattice ($\mathbf{k}=0$), we could obtain the two-dimensional discrete NLS (DNLS) equation. Furthermore, solitons could be obtained corresponding to gaps in the Brillouin zones.

The system of Eqs. (15) and (16) is the discrete Dirac system. In this paper we focus on the continuous problem. Taking the continuum limit of the discrete Dirac system, after some straightforward calculations, we obtain the governing equation for a,

$$i\frac{\partial a}{\partial z} - \mu_{0,0}a - \frac{\sqrt{3}}{2}\epsilon\mu_{0,0}(\partial_x b - i\partial_y b) + g\sigma|a|^2 a = 0, \quad (17)$$

similarly, the b equation has the form

$$i\frac{\partial b}{\partial z} - \mu_{0,0}b + \frac{\sqrt{3}}{2}\epsilon\mu_{0,0}(\partial_x a + i\partial_y a) + g\sigma|b|^2 b = 0. \quad (18)$$

Notice that $\mu_{0,0}a$ and $\mu_{0,0}b$ can be absorbed into the first terms by defining new variables $\tilde{a}=ae^{-i\mu_{0,0}z}$ and $\tilde{b}=be^{-i\mu_{0,0}z}$ (we drop the tildes below). Letting $D=-\frac{\sqrt{3}}{2}\epsilon\mu_{0,0}$ we finally get the continuous nonlinear Dirac system

$$i\frac{\partial a}{\partial z} + D(\partial_- b) + g\sigma|a|^2 a = 0, \quad (19)$$

$$i\frac{\partial b}{\partial z} - D(\partial_+ a) + g\sigma|b|^2 b = 0, \quad (20)$$

where $\partial_\pm = \partial_x \pm i\partial_y$.

Thus the evolution of envelopes of Bloch modes associated with the lattice NLS equation near a diabolical point are governed, in general, by a nonlinear Dirac system. If $\sigma=0$, one gets the linear Dirac system; but if $\sigma\neq 0$, one gets the nonlinear Dirac system. Let us consider the linear system first. The dispersion relation for the linear system is defined by the equation

$$\begin{pmatrix} -\omega & D(ik_x + k_y) \\ D(-ik_x + k_y) & -\omega \end{pmatrix}\begin{pmatrix} \hat{a} \\ \hat{b} \end{pmatrix} = \begin{pmatrix} 0 \\ 0 \end{pmatrix}, \quad (21)$$

so the dispersion relation is

$$\omega^2 = D^2(k_x^2 + k_y^2). \quad (22)$$

This is a cone and this cone is exactly the dispersion relation of the honeycomb lattice near the diabolical point $K=(0,\frac{4\pi}{3\sqrt{3}l})$.

The envelopes of the Bloch modes near the diabolical point K disperse conically in the honeycomb lattices. This phenomenon can be described by the Dirac system (19) and (20). We know that there are two sets of opposite diabolical points which are equivalent to K and K'. The above derivation is for $K=(0,\frac{4\pi}{3\sqrt{3}l})$. If we choose the other diabolical point $K'=(0,\frac{8\pi}{3\sqrt{3}l})$, the analysis is exactly the same as well as the dispersion relation. However, the corresponding system becomes

$$i\frac{da}{dz} + D(\partial_+ b) + g\sigma|a|^2 a = 0, \quad (23)$$

$$i\frac{db}{dz} - D(\partial_- a) + g\sigma|b|^2 b = 0. \quad (24)$$

The only difference is just a variable change, $y\to -y$.

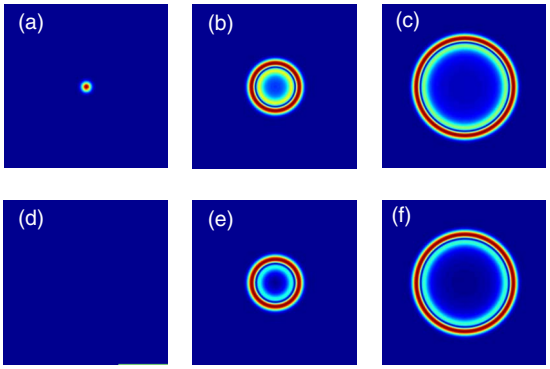

FIG. 4. (Color online) Simulations of the Dirac Eqs. (19) and (20) with $\sigma=0$. The initial conditions are that a is a Gaussian and b is zero. (a)–(c) Intensities of the a component at time 0, 5.4, and 10.8; (d)–(f) intensity of the b component at time 0, 5.4, and 10.8.

V. SIMULATIONS OF THE DIRAC SYSTEM AND COMPARISONS

In Sec. IV, we derive the evolution equations for the envelope of Bloch modes near a diabolical point which results in the Dirac system. Next, we demonstrate the derivation by numerical comparisons. The numerical method we use to solve the Dirac system is the same as the one we used for the NLS equation in Sec. III. In Fig. 2, we simulated the linear lattice NLS equations, i.e., $\sigma=0$. So the corresponding Dirac system is linear. We simulate the linear Dirac system with two sets of initial conditions. The results are displayed in Figs. 4 and 5. In Fig. 4, a is a unit Gaussian and b is zero initially. The intensities of both a and b are two perfect rings and the width of the rings does not change. This is consistent with the conical diffraction phenomenon which we observed in Fig. 2 (upper row) and Peleg *et al.* [6] observed in their experiments. On the other hand in Fig. 5, both a and b initially are unit Gaussians. The intensities of a and b have different ring structures from before in Fig. 4. Now the rings have notches at the bottom which correspond to the "half-turn polarization" which we observed in direct lattice NLS equation simulations [see Fig. 2 (lower row)]. The conical

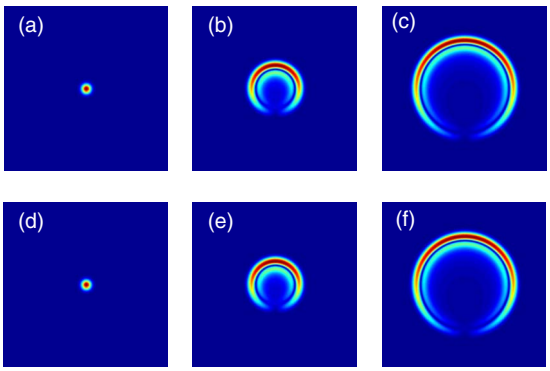

FIG. 5. (Color online) Simulations of Dirac Eqs. (19) and (20) with $\sigma=0$. The initial conditions here are that a and b are the same Gaussian. (a)–(c) depict intensities of the a component at time 0, 5.4, and 10.8; and (d)– (f) depict the b component at time 0, 5.4, and 10.8.

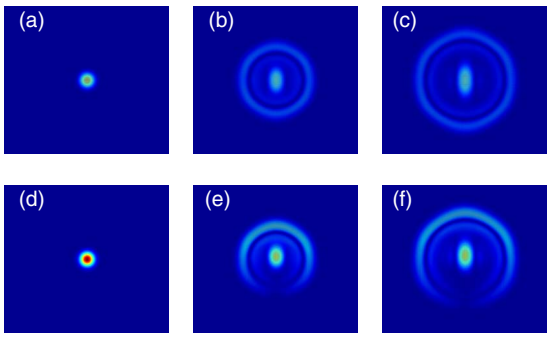

FIG. 6. (Color online) The propagation of light beams in a saturablelike lattice—see Eq. (25); (a)–(c) two plane waves; (d)–(f) one plane wave, each multiplied by a Gaussian envelope

diffraction in the Dirac system agrees well with that in the original lattice NLS equation. So the Dirac system is the proper system to describe this interesting phenomenon.

It is also useful to compare our analysis with previous interesting studies [6]. Thus we also simulated the saturable lattice NLS equation,

$$i\psi_z + \nabla^2\psi + \frac{E_0}{1 + V(\mathbf{r}) + \sigma|\psi|^2}\psi = 0, \tag{25}$$

where $V(\mathbf{r})$ has the form in Eq. (2). In this case, we choose $\sigma=0$, $V_0=1$, and $E_0=1000$. Launching two different initial beams which are the same as before, we get evolution results which are displayed in Fig. 6. The evolution patterns are similar to the patterns in Fig. 2 except there is a central spot

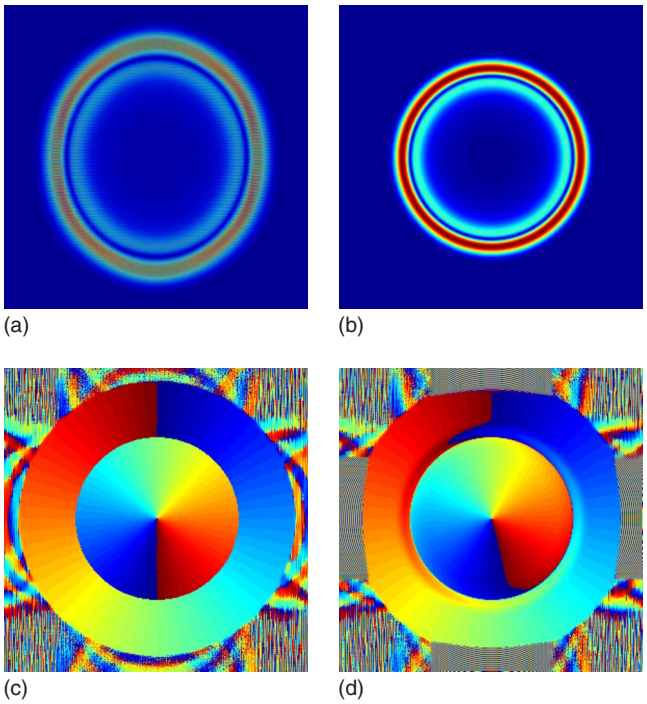

FIG. 7. (Color online) Simulations of (a) the nonlinear lattice equation and (b) the nonlinear Dirac system. The comparison of the phases in the simulations of both (c) linear and (d) nonlinear Dirac systems.

with the saturable potential. Peleg *et al.* [6] claimed that the central spot comes from higher band components which do not disperse conically. The above analysis can be applied to Eq. (25) and (apart from coefficient values) a Dirac system will be obtained. Hence one expects and finds that the main features in the evolution of the envelopes in both a linear potential lattice and the saturable potential lattice are similar since they are governed by the Dirac system. Details will be further investigated in the future.

From the simulations and analysis, we obtained conical diffraction associated with the linear lattice. However we also note that the essentials of conical diffraction also exist in the presence of the lattice nonlinearity. We simulate the original lattice Eq. (1) with $\sigma=1$ and find that the evolution of the intensities are almost the same as the linear case where $\sigma=0$. A typical pattern is displayed in Fig. 7(a) (nonlinear) which corresponds to Fig. 2(c) (linear). We also simulate the nonlinear Dirac system derived above, and the evolution of the intensities is found to be almost the same as the linear case. A typical pattern is displayed in Fig. 7(b) (nonlinear) which can be compared with Fig. 4(c) (linear). So, conical diffraction not only exists in the linear regime but is also a nonlinear phenomenon as well. The nonlinear Dirac system properly describes this phenomenon. While the evolution of the intensities for both linear and nonlinear Dirac systems is essentially unchanged, the phases in linear and nonlinear systems are different [see Figs. 7(c) and 7(d)]. A detailed analysis is outside the scope of this paper.

VI. CONCLUSIONS AND DISCUSSIONS

In this paper conical diffraction in honeycomb lattices is analyzed. In the tight-binding limit, a discrete and continuous Dirac system of evolution equations for the envelopes of two sublattice Bloch modes near the diabolical points is derived directly from the lattice NLS equation. This Dirac system yields the same evolution patterns as in lattice NLS equations. Thus the tight-binding limit contains the underlying mechanism of conical diffraction in honeycomb lattices. It is also found that conical diffraction survives in the presence of nonlinearity. While numerical simulations indicate that the nonlinearity only affects the phase, a detailed theory still needs to be developed. It is also of interest to consider other periodic potentials which might have diabolical points where this and related theories could be applied.

ACKNOWLEDGMENTS

The authors thank O. Bahat-Treidel and O. Peleg for useful information about their work and Professor J. Yang for valuable suggestions. This research was partially supported by the U.S. Air Force Office of Scientific Research under Grant No. FA4955-06-1-0237 and by the National Science Foundation under Grant No. DMS-0505352.

[1] W. R. Hamilton, Trans. Royal Irish Acad. **17**, 1 (1837).
[2] H. Lloyd, Trans. Royal Irish Acad. **17**, 145 (1837).
[3] M. V. Berry and M. R. Jeffrey, Prog. Opt. **50**, 13 (2007).
[4] M. V. Berry, M. R. Jeffrey, and J. G. Lunney, Proc. R. Soc. London, Ser. A **462**, 1629 (2006).
[5] R. A. Indik and A. C. Newell, Opt. Express **14**, 10614 (2006).
[6] O. Peleg *et al.*, Phys. Rev. Lett. **98**, 103901 (2007).
[7] O. Bahat-Treidel *et al.*, Opt. Lett. **33**, 2251 (2008).
[8] C. R. Rosberg *et al.*, Opt. Lett. **32**, 397 (2007).
[9] P. R. Wallace, Phys. Rev. **71**, 622 (1947).
[10] K. S. Novoselov *et al.*, Science **306**, 666 (2004).
[11] K. v. Klitzing, G. Dorda, and M. Pepper, Phys. Rev. Lett. **45**, 494 (1980).
[12] R. Jackiw and C. Rebbi, Phys. Rev. D **13**, 3398 (1976).
[13] S. Raghu and F. D. M. Haldane, Phys. Rev. A **78**, 033834 (2008).
[14] F. D. M. Haldane and S. Raghu, Phys. Rev. Lett. **100**, 013904 (2008).
[15] L. H. Haddad and L. D. Carr, Physica D (to be published).
[16] W. Fushchich and R. Zhdanov, *Symmetries and Exact Solutions of Nonlinear Dirac Equations* (Mathematical Ukraina, Ukraine, 1997).
[17] N. K. Efremidis, J. Hudock, D. N. Christodoulides, J. W. Fleischer, O. Cohen, and M. Segev, Phys. Rev. Lett. **91**, 213906 (2003).
[18] M. Notomi, Phys. Rev. B **62**, 10696 (2000).
[19] G. L. Alfimov *et al.*, Phys. Rev. E **66**, 046608 (2002).